Intermediate valence to heavy fermion through a quantum phase transition in $Yb_3(Rh_{1-x}T_x)_4Ge_{13}$ (T = Co, Ir) single crystals

Binod K. Rai,[1] Iain W. H. Oswald,[2] Julia Y. Chan,[2] and E. Morosan[1]
[1]*Department of Physics and Astronomy, Rice University, Houston, Texas 77005, USA*
[2]*Department of Chemistry, University of Texas at Dallas, Richardson, Texas 75080, USA*
(Received 23 September 2015; published 4 January 2016)

Single crystals of $Yb_3(Rh_{1-x}T_x)_4Ge_{13}$ (T = Co, Ir) have been grown using the self-flux method. Powder x-ray diffraction data on these compounds are consistent with the cubic structure with space group $Pm\bar{3}n$. Intermediate-valence behavior is observed in $Yb_3(Rh_{1-x}T_x)_4Ge_{13}$ upon T = Co doping, while T = Ir doping drives the system into a heavy-fermion state. Antiferromagnetic order is observed in the Ir-doped samples $Yb_3(Rh_{1-x}T_x)_4Ge_{13}$ for $0.5 < x \leqslant 1$ with $T_N = 0.96$ K for $Yb_3Ir_4Ge_{13}$. With decreasing x, the magnetic order is suppressed towards a quantum critical point around $x_c = 0.5$, accompanied by non-Fermi-liquid behavior evidenced by logarithmic divergence of the specific heat and linear temperature dependence of the resistivity. The Fermi-liquid behavior is recovered with the application of large magnetic fields.

DOI: 10.1103/PhysRevB.93.035101

I. INTRODUCTION

Valence instabilities have often been observed in rare-earth compounds with nearly full or empty $4f$ shells. Therefore, compounds with Ce or Yb can be tuned with extrinsic parameters such as pressure, magnetic field, or doping, resulting in a variety of states such as heavy fermion (HF) [1–3], superconductivity [4], intermediate valence [5], and mixed valence [6,7]. While existing literature often uses intermediate- and mixed-valence terminology interchangeably, these actually refer to two distinct behaviors: temperature-dependent or temperature-independent mixtures of both magnetic and nonmagnetic rare-earth ions. In this paper the focus is on the temperature-dependent scenario, denoted as intermediate valence. Intermediate-valence compounds can be tuned to a HF state with the application of pressure or doping, which effectively shifts the $4f$ energy level relative to the conduction band [8–11]. In turn, the magnetic order in some HF systems can be suppressed towards a quantum critical point (QCP), often accompanied by non-Fermi-liquid (NFL) behavior [12–18].

Compounds with the stoichiometry $A_3T_4M_{13}$ (3-4-13) (A is a rare-earth or alkaline-earth element, T is a transition metal, and M is a group-14 element) exhibit diverse properties such as magnetism and superconductivity [19–22], structural phase transitions [23], and intermediate-valence behavior [24,25]. A few Ce-based 3-4-13 compounds are reported as being paramagnetic (PM) HFs ($Ce_3Co_4Sn_{13}$ [26,27] and $Ce_3Rh_4Sn_{13}$ [28]) or magnetically ordered HFs ($Ce_3Pt_4In_{13}$ [29] and $Ce_3Ir_4Sn_{13}$ [30,31]). However, no Yb-based 3-4-13 PM or magnetically ordered HFs are known to date. Polycrystalline $Yb_3T_4Ge_{13}$ (T = Ir, Rh) compounds have been reported to order antiferromagnetically around $T_N = 2.3$ K [32,33], a temperature very close to that of the magnetic order in Yb_2O_3. In this study on single crystals of $Yb_3(Rh_{1-x}T_x)_4Ge_{13}$, we present evidence that the $x = 1$, T = Ir compound is an antiferromagnetic HF with $T_N = 0.96$ K, while the $x = 0$ analog shows intermediate-valence behavior. Furthermore, the intermediate valence was found to persist with T = Co doping up to $x = 1$, while T = Ir doping changes the system from intermediate valence to heavy fermion around $x = 0.25$. Additionally, the magnetic order in $Yb_3(Rh_{1-x}Ir_x)_4Ge_{13}$ is suppressed towards a QCP around a critical Ir composition $x_c = 0.5$, accompanied by NFL behavior at $H = 0$. Since no 2.3 K transition was observed in single crystals of $Yb_3(Rh_{1-x}T_x)_4Ge_{13}$ (T = Co, Ir) without prolonged air exposure, it is possible that the earlier reported polycrystalline samples displayed the Yb_2O_3 transition caused by surface oxidation in air.

II. METHODS

Single crystals of $Yb_3(Rh_{1-x}T_x)_4Ge_{13}$ (T = Co, Ir) were prepared using a self-flux method as discussed elsewhere [34]. Powder x-ray diffraction patterns were collected at $T = 300$ K in a Rigaku D/Max x-ray diffractometer using Cu $K\alpha$ radiation. Rietveld analysis was performed using the GSAS software package [35]. The dc magnetic susceptibility was measured in a Quantum Design (QD) Magnetic Properties Measurement System (MPMS) with an iHelium ^{3}He option, with the magnetic field $H \| a$. Heat-capacity data were collected in a QD Physical Properties Measurement System (PPMS) with a ^{3}He insert using an adiabatic thermal relaxation method. The temperature-dependent ac resistivity of bar-shaped crystals was measured in the QD PPMS, with the current $i \| a$, $i = 1$ mA, $f = 17.77$ Hz.

III. RESULTS AND ANALYSIS

Rietveld analysis of the powder x-ray diffraction pattern of $Yb_3(Rh_{1-x}T_x)_4Ge_{13}$ (T = Co, Ir) confirms the cubic structure with space group $Pm\bar{3}n$ [34]. Figure 1(a) displays an example of a powder diffraction pattern for $x = 0$, with asterisks marking a minute amount of Ge flux. Figure 1(b) (solid symbols) shows the variation in the experimental lattice parameter a as a function of x, with x increasing to the left (right) for dopant T = Co (Ir). With Co doping, a small lattice contraction is observed in $Yb_3(Rh_{1-x}Co_x)_4Ge_{13}$, resulting from the fact that relatively bigger Rh atoms ($r_{Rh} = 0.66$ Å) are replaced by smaller Co atoms ($r_{Co} = 0.58$ Å) [36]. A much smaller change in a is registered for Ir doping in $Yb_3(Rh_{1-x}Ir_x)_4Ge_{13}$ given that the Ir ionic radius

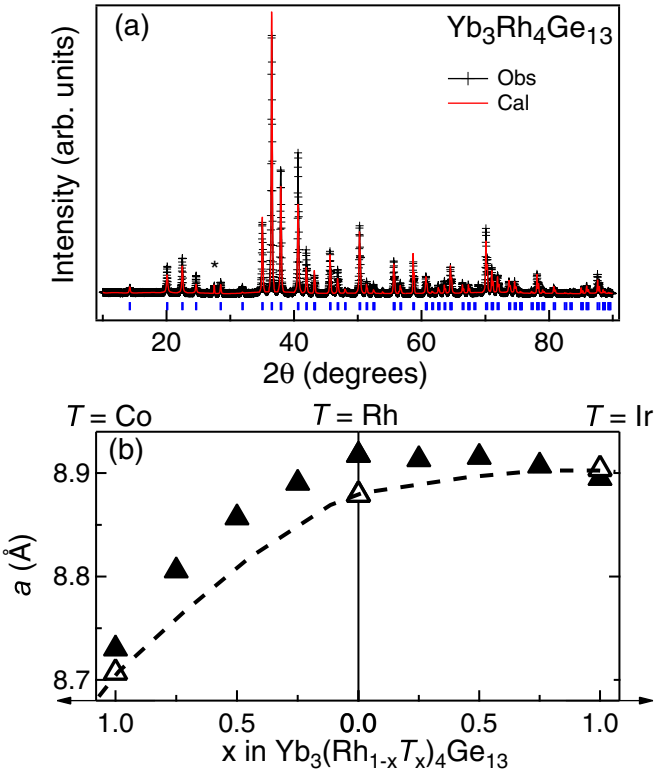

FIG. 1. (a) Room-temperature measured (symbols) and calculated (observed) powder x-ray diffraction pattern for $Yb_3Rh_4Ge_{13}$, together with the calculated peak positions (blue vertical lines). A minute amount of Ge flux is marked with an asterisk. (b) Experimental (solid) and estimated (open) lattice parameters for $Yb_3(Rh_{1-x}T_x)_4Ge_{13}$ as a function of x (solid triangles). The open triangles correspond to the lattice parameters for the trivalent Yb compounds estimated from the lanthanide contraction extrapolation between the R = Tm and Lu $R_3T_4Ge_{13}$ compounds.

($r_{Ir} = 0.68$ Å) is very close to that of Rh. However, a comparison of the measured lattice parameters (solid symbols) with the expected values (open symbols) for the Yb^{3+} compounds is very informative. The open symbols correspond to lattice parameter values calculated using the expected Lanthanide contraction [36] across the $R_3T_4Ge_{13}$ series with R = Tm, Yb, Lu (T = Co, Rh, Ir). For each T, the reported a values for R = Tm and Lu [34,37] were used to determine the expected parameter for the R = Yb trivalent analog. For example, for the $Yb_3Ir_4Ge_{13}$ sample, the expected value was linearly interpolated from the lattice parameters of $Tm_3Ir_4Ge_{13}$ [37] and $Lu_3Ir_4Ge_{13}$[34]. From Fig. 1(b), it is readily apparent that Yb is likely in a trivalent state in the T = Ir compounds, while the deviation from the expected lattice parameter for R^{3+} in the T = Co and Rh compounds implies that the Yb ion is in a mixed (less then trivalent) or intermediate (temperature-dependent) valence state. This is indeed consistent with magnetization and transport data presented below.

The temperature-dependent magnetic susceptibility for $Yb_3(Rh_{1-x}Co_x)_4Ge_{13}$, shown in Fig. 2(a), reveals a broad maximum above ~150 K, a typical feature of intermediate-valence systems. According to the interconfiguration-fluctuation (ICF) model [38], the rare-earth Yb can fluctuate between the

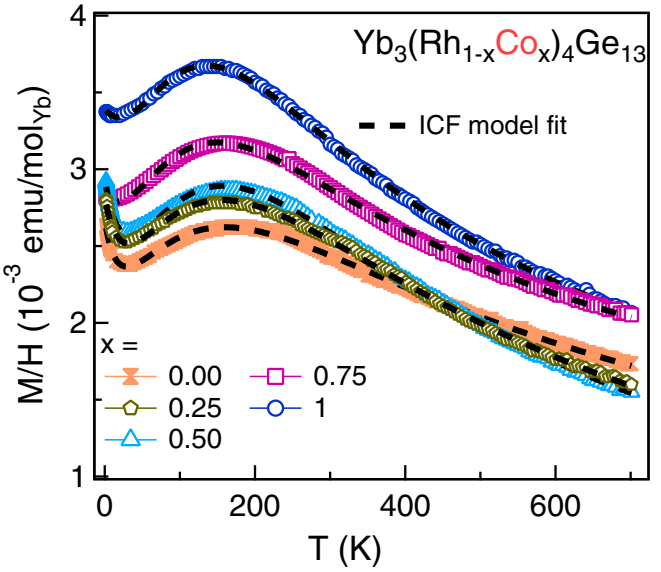

FIG. 2. Temperature-dependent magnetic susceptibility M/H for H = 0.1 T of $Yb_3(Rh_{1-x}Co_x)_4Ge_{13}$ together with the ICF model fit (dashed lines).

nonmagnetic $4f^{14}$ ($J = 0$ and $\mu_{\rm eff} = 0$) and magnetic $4f^{13}$ ($J = 7/2$ and $\mu_{\rm eff} = 4.54\,\mu_B$) ground states. The ICF magnetic susceptibility is of the form [38–40]

$$\chi(T) = \chi(0) + \frac{C'}{T+\theta} + \frac{8N_A(4.54\mu_B)^2}{3k_BT\left(1+\frac{T_{sf}}{T}\right)\left[8+e^{\frac{E_{ex}}{k_BT\left(1+\frac{T_{sf}}{T}\right)}}\right]},$$

where C' and θ are the Curie-Weiss constant and Weiss temperature associated with the small fraction of Yb^{3+} ions, E_{ex} is the energy gap between the magnetic and nonmagnetic configurations, and T_{sf} is the spin-fluctuation temperature related to the rate of valence fluctuation between 2+ and 3+ states. The fit values for C', θ, E_{ex}, and T_{sf} are shown in Table I. Both E_{ex} and T_{sf} decrease, while C' increases with increasing Co concentration in $Yb_3(Rh_{1-x}Co_x)_4Ge_{13}$, consistent with the departure from the intermediate-valence state with increasing x. This was already suggested by the difference between the experimental (solid) and calculated (open) lattice parameters for the trivalent Yb compounds seen in Fig. 1(b).

By contrast, Ir doping rapidly drives $Yb_3(Rh_{1-x}Ir_x)_4Ge_{13}$ towards the trivalent, local-moment Yb limit: even for $x = 0.25$, the broad maximum caused by intermediate valence disappears, as shown in Fig. 3(a), and instead, the magnetic susceptibility has a Curie-Weiss temperature dependence. The

TABLE I. Parameters for $Yb_3(Rh_{1-x}T_x)_4Ge_{13}$ (T = Co) from ICF model fits.

x	E_{ex}/k_B (K)	T_{sf} (K)	$\chi(0)$(emu/mol$_{Yb}$)	θ (K)	C'
0.00	810(11)	208(7)	0.00011(3)	28(2)	0.037(4)
0.25	780(11)	180(9)	0.00036(6)	47(5)	0.098(1)
0.50	740(9)	155(7)	0.00045(1)	52(4)	0.13(1)
0.75	671(1)	122(1)	0.00060(1)	110(1)	0.28(1)
1.00	621(1)	94(1)	0.00030(1)	262(1)	0.74(1)

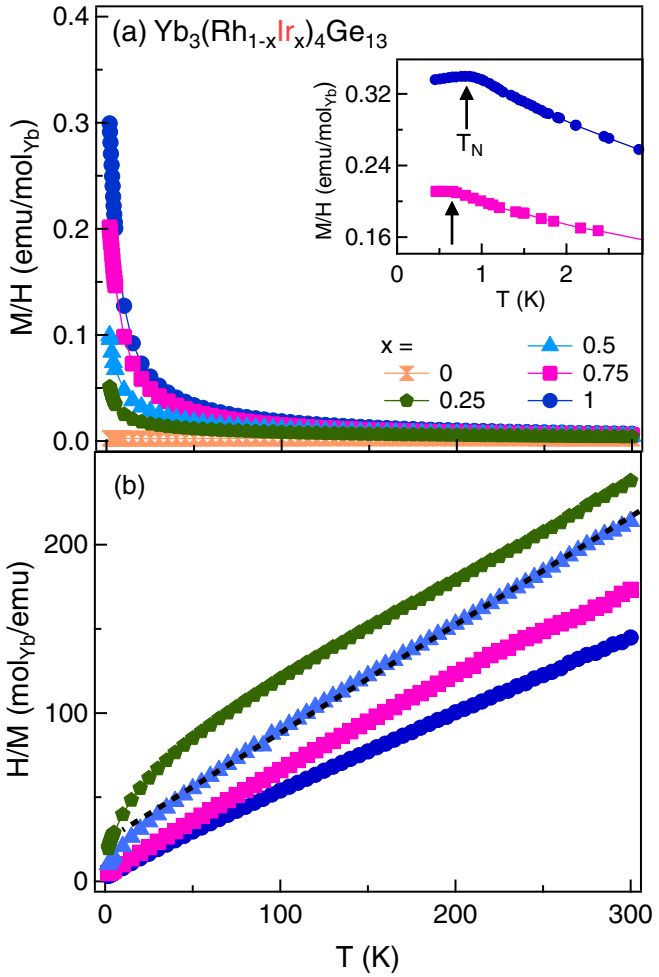

FIG. 3. (a) Temperature-dependent magnetic susceptibility M/H of $Yb_3(Rh_{1-x}Ir_x)_4Ge_{13}$ for $H = 0.1$ T. Inset: low-temperature M/H showing the antiferromagnetic ordering temperature T_N marked by vertical arrows. (b) Inverse magnetic susceptibility H/M vs T for $Yb_3(Rh_{1-x}Ir_x)_4Ge_{13}$ at $H = 0.1$ T, with an example of a Curie-Weiss fit (dotted line).

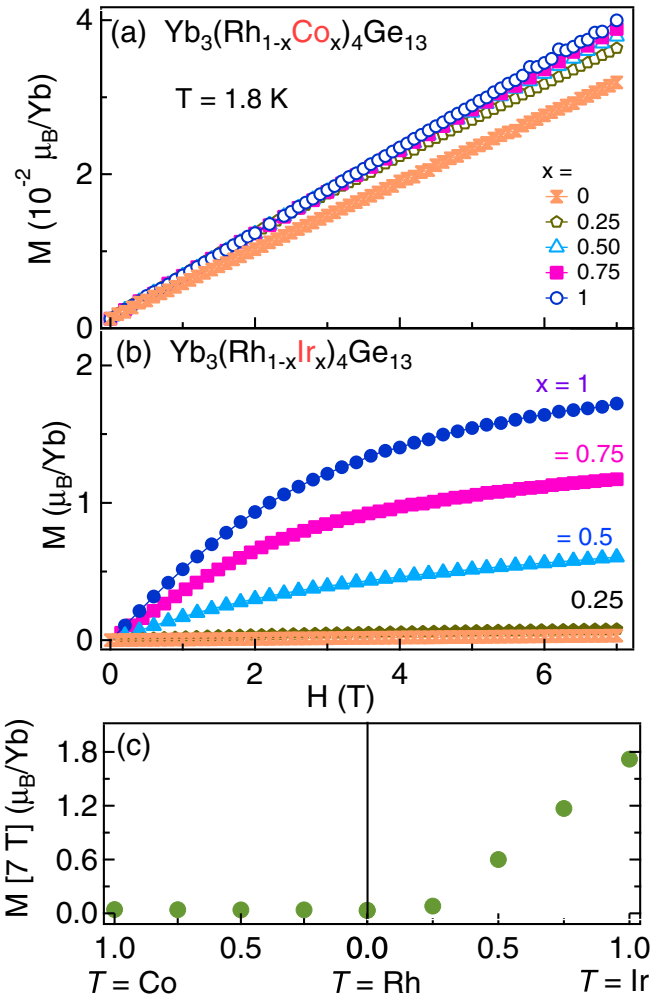

FIG. 4. $M(H)$ isotherms at $T = 1.8$ K for $Yb_3(Rh_{1-x}T_x)_4Ge_{13}$ with (a) $T =$ Co and (b) $T =$ Ir. (c) The $Yb_3(Rh_{1-x}T_x)_4Ge_{13}$ magnetic moment at $H = 7$ T and T = 1.8 K as a function of x.

effective moment values μ_{eff} and Weiss temperatures θ determined from the Curie-Weiss fits of the inverse susceptibility [Fig. 3(b)] are listed in the Table II. As x approaches 1 in $Yb_3(Rh_{1-x}Ir_x)_4Ge_{13}$, the effective moment increases towards the theoretical value for trivalent Yb ($\mu_{\text{eff}} = 4.54\mu_B$/Yb). A cusp in the magnetic susceptibility [inset of Fig. 3(a)] for the $x = 0.75$ and 1.00 samples signals antiferromagnetic order below $T = 0.57$ K ($x = 0.75$) and $T = 0.96$ K ($x = 1.00$).

TABLE II. Parameters for $Yb_3(Rh_{1-x}T_x)_4Ge_{13}$ (T = Ir) from Curie-Weiss fits.

x	μ_{eff} (μ_B/Yb)	θ (K)
0.25	3.7	101
0.50	3.6	49
0.75	3.8	24
1.00	4.2	17

A comparison of the field-dependent magnetization isotherms for the Co- and Ir-doped $Yb_3Rh_4Ge_{13}$ reinforces the observations from the temperature-dependent magnetic susceptibility: for $Yb_3(Rh_{1-x}Co_x)_4Ge_{13}$, $M(H)$ at $T = 1.8$ K [Fig. 4(a)] remains very small and linear. At low temperature ($T = 1.8$ K), the Ir-doped samples [Fig. 4(b)] display increasing $M(H)$ values with increasing x. However, the maximum at the highest measured field μ[7 T; 1.8 K] is still substantively lower than the saturated Yb^{3+} moment $\mu_{sat} = 4\mu_B$. The μ[7 T; 1.8 K] values for all $Yb_3Rh_4Ge_{13}$-doped samples are summarized in Fig. 4(c), illustrating the transition from intermediate-valence behavior to a magnetic state around $x = 0.25$ in $Yb_3(Rh_{1-x}Ir_x)_4Ge_{13}$.

The specific-heat data reveal that this magnetic state corresponds to heavy-fermion behavior in the Ir-doped $Yb_3Rh_4Ge_{13}$. The electronic specific-heat coefficient $\gamma = C_p/T|_{T=0}$ for $Yb_3(Rh_{1-x}Co_x)_4Ge_{13}$ (Fig. 5) ranges from 35 to 55 mJ/mol$_{Yb}$K^2, consistent with other intermediate-valence compounds [39,41,42]. On the other hand, the Ir-doped series shows large electron mass renormalization (Fig. 6), with $\gamma > 1.2$ J/mol K^2 for $x = 0.50$. Upon approaching this

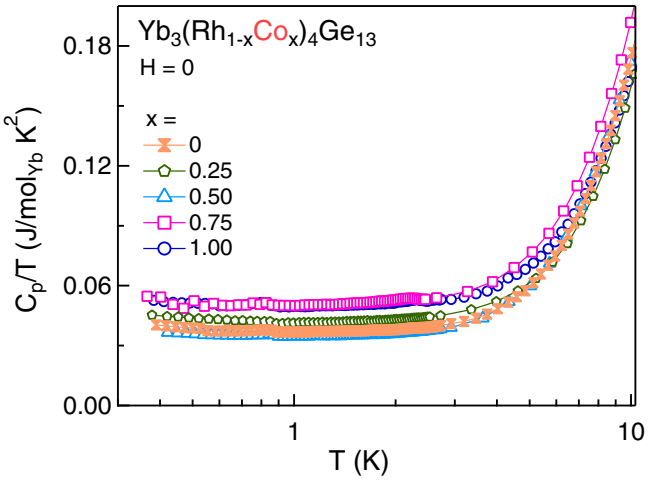

FIG. 5. $H = 0$ $Yb_3(Rh_{1-x}Co_x)_4Ge_{13}$ specific heat scaled by temperature C_p/T.

composition from the $x = 1$ limit, the magnetic order at $T_N = 0.96$ K in $Yb_3Ir_4Ge_{13}$ is suppressed below 0.35 K, indicative of a QCP around $x = 0.5$. At the critical composition, the $H = 0$ specific heat scaled by temperature C_p/T

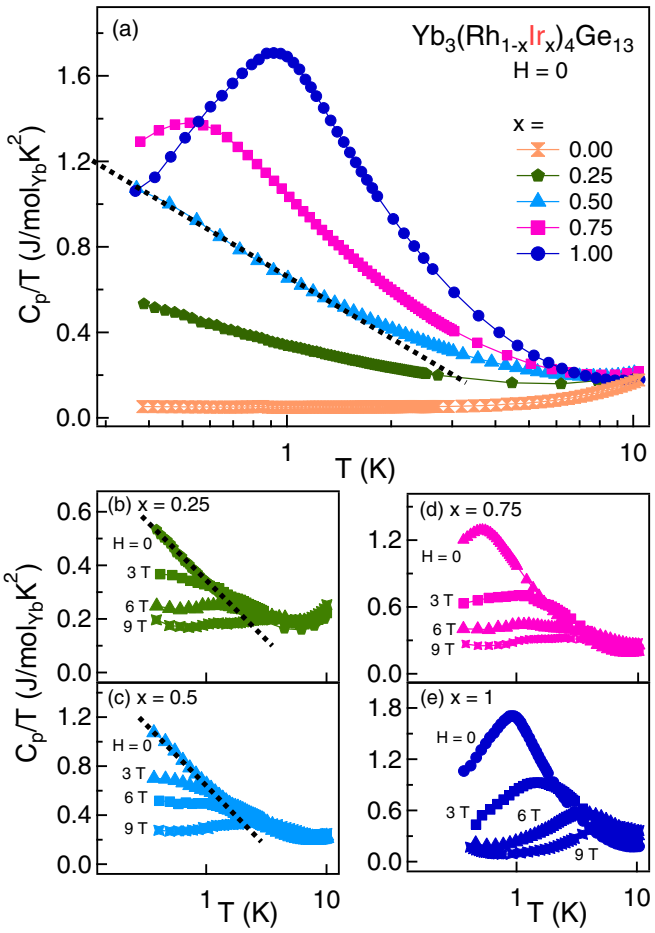

FIG. 6. (a) $Yb_3(Rh_{1-x}Ir_x)_4Ge_{13}$ C_p/T vs T for $H = 0$. C_p/T vs T in applied magnetic field H for (b) $x = 0.25$, (c) $x = 0.50$, (d) $x = 0.75$, and (e) $x = 1.0$.

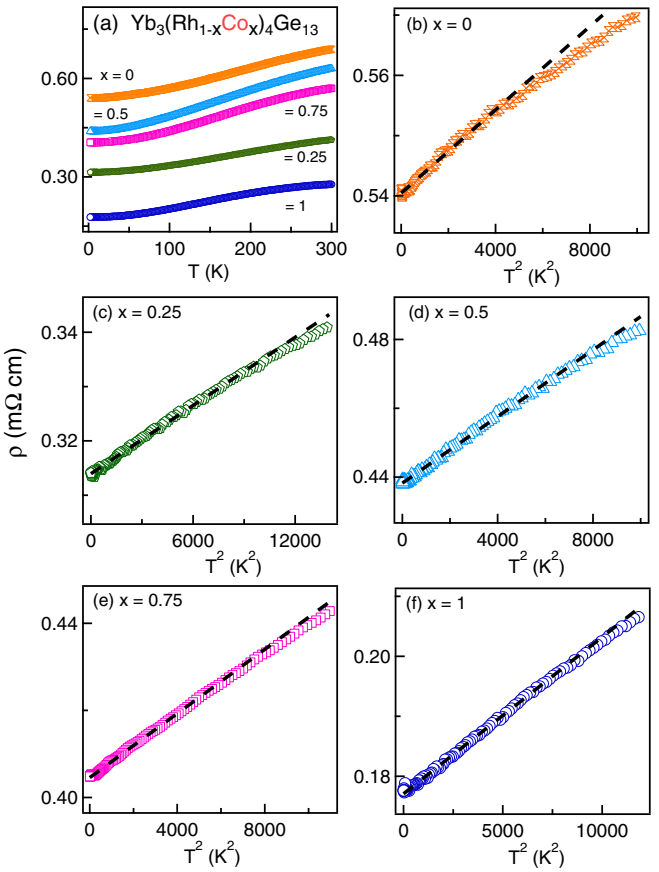

FIG. 7. (a) $H = 0$ temperature-dependent electrical resistivity of $Yb_3(Rh_{1-x}Co_x)_4Ge_{13}$. (b)–(f) $H = 0$, $\rho(T)$ vs T^2 (symbols) together with the $\rho(T) = \rho_o + AT^2$ fits (dashed lines).

[Fig. 6(a)] displays logarithmic divergence ranging over nearly a decade in temperature (dotted line). This is a signature of non-Fermi-liquid behavior often observed in the quantum critical regime of HF compounds [12,42–45]. The application of the magnetic field restores the Fermi-liquid behavior for $H > 3$ T [Figs. 6(b)–6(d)] for samples with low Ir content ($x = 0.25, 0.5$ and $x = 0.75$). However, for the highest Ir content [Fig. 6(e)], the peak at T_N moves up in temperature and broadens with increasing magnetic fields. Such behavior is often observed in HF compounds [44,46,47], and it is attributed to the magnetic entropy increase with increasing field, caused by the modification of local-moment intersite interactions [46,47].

To further verify the NFL regime in $Yb_3(Rh_{1-x}T_x)_4Ge_{13}$, the electrical resistivity was measured and is shown in Figs. 7 and 8. Consistent with the specific-heat data, as well as with other intermediate-valence systems [39,41,42], the $H = 0$ electrical resistivity of the Co-doped series [Fig. 7(a)] shows no anomaly and a weak metallic temperature dependence. The $Yb_3(Rh_{1-x}Co_x)_4Ge_{13}$ samples ($0 \leqslant x \leqslant 1$) display Fermi-liquid behavior, marked by the quadratic temperature dependence of the resistivity [Figs. 7(b)–7(f)] at low temperatures. Conversely, in the Ir doping the Fermi-liquid (FL) signatures are clouded by the emergent Kondo behavior common to HFs [4,12,29,48], reflected in the local maxima that develop in $\rho(T)$ starting at $x = 0.25$ [symbols, Figs. 8(a)–8(d)]. This

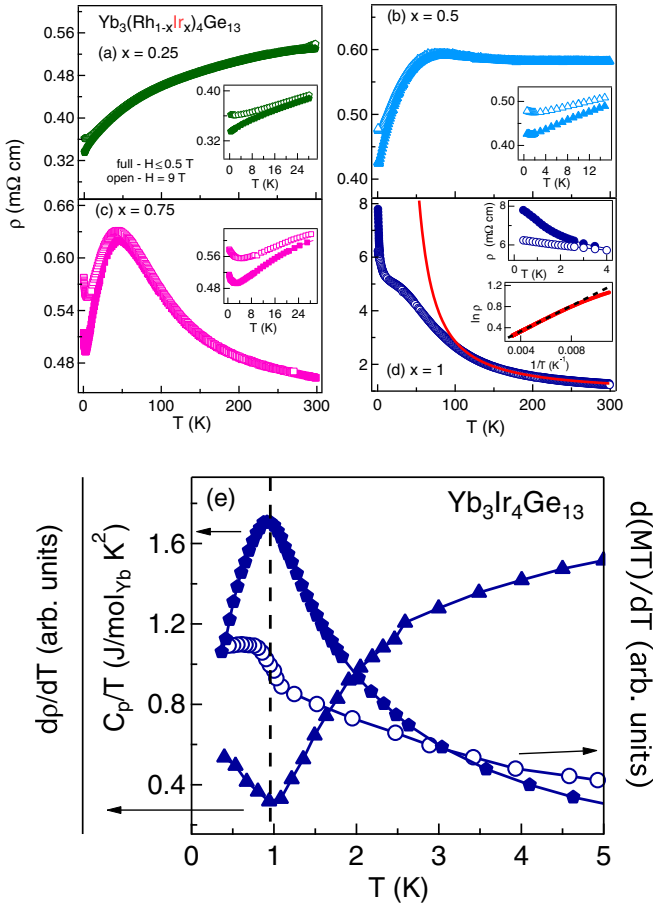

FIG. 8. (a)–(d) $H \leqslant 0.5$ (solid) and 9 T (open) temperature-dependent electrical resistivity for $Yb_3(Rh_{1-x}Ir_x)_4Ge_{13}$. Insets: low-temperature resistivity range. The solid line in (d) represents the high-temperature fit to an activated resistivity $\rho(T) = \rho_0 e^{E_g/k_B T}$, with E_g determined from the linear fit of $\ln\rho$ vs $1/T$ (dashed line, bottom inset), $E_g/k_B = 120$ K. (e) The ordering temperature T_N (vertical dashed line) for $Yb_3Ir_4Ge_{13}$ determined from peaks in C_p/T ($H = 0$, pentagons, left axis), $d(MT)/dT$ ($H = 0.1$ T, circles, right axis), and a minimum in the resistivity derivative ($H = 0$, triangles, very left axis).

local maximum becomes more pronounced with increasing x, as the overall resistivity values increase, and the metallic behavior is replaced by a semiconducting-like temperature dependence in $Yb_3Ir_4Ge_{13}$ [Fig. 8(d)]. To examine whether the semiconducting behavior of $Yb_3Ir_4Ge_{13}$ is due to disorder as is the case in the 3-4-13 germanides [34], room-temperature single-crystal x-ray diffraction measurements were performed for the three parent compounds $Yb_3T_4Ge_{13}$ (T = Co, Rh, and Ir). While $Yb_3Rh_4Ge_{13}$ and $Yb_3Co_4Ge_{13}$, showing poor metallic resistivity [Fig. 7(a)], have atomic displacement parameter (ADP) ratios of 3.98 and 3.54, respectively, $Yb_3Ir_4Ge_{13}$ crystals have a large ADP ratio of 4.88, a value well within the range of other reported semiconducting 3-4-13 germanides [34]. This suggests that disorder is at play in $Yb_3Ir_4Ge_{13}$, and indeed, the high-temperature resistivity [symbols, Fig. 8(d)] can be fit to an activated resistivity $\rho(T) = \rho_0 e^{E_g/k_B T}$ [solid line, Fig. 8(d)]. The linear fit (dashed line) of the semilog plot $\ln\rho$ vs 1/T [bottom inset, Fig. 8(d)] yields a small gap

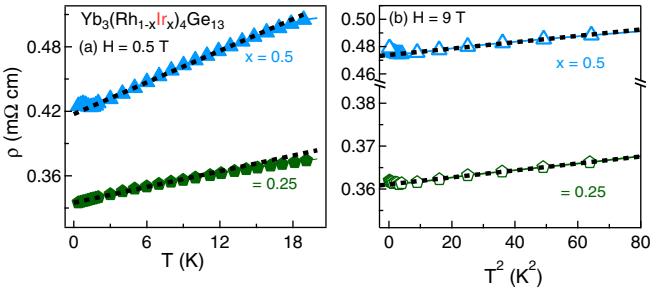

FIG. 9. (a) $\rho(T)$ vs T and (b) $\rho(T)$ vs T^2 (symbols), together with linear fits (dotted lines).

value $E_g/k_B \approx 120$ K. However, clear deviations from the semiconducting behavior occur at low temperatures (below ~100 K). Together with the large $C_p/T \approx 1$ J/mol K^2, the low-temperature deviation from the exponential resistivity suggests that the transport properties of $Yb_3Ir_4Ge_{13}$ are likely a convolution of large ADP and Kondo behavior.

The magnetic order in $Yb_3Ir_4Ge_{13}$ is marked by a sharp increase in the $H = 0$ $\rho(T)$, which corresponds to a minimum in the resistivity derivative $d\rho(T)/dT$ at $T_N = 0.96$ K [triangles, Fig. 8(e)]. Not surprisingly, this transition temperature is consistent with the value determined from the magnetization derivative $d(MT)/dT$ [49] and C_p/T, as illustrated for $x = 1$ in Fig. 8(e) (pentagons and circles, respectively). At lower compositions ($x \leqslant 0.5$), a resistivity drop occurs around $T = 1$ K (not shown) in the Ir-doped series ($x = 0.25$ and 0.5), of as yet unknown origin. The drop in the resistivity at lower temperature was less than 9%. While a superconducting transition just above 0.4 K cannot be ruled out, no corresponding signatures were visible in the low-field susceptibility data ($H = 5$ Oe, not shown) or zero-field specific-heat data (Fig. 6), both measured down to 0.4 K. A small magnetic field ($H = 0.5$ T) suppresses the drop in resistivity, and the resulting $H = 0.5$ T low-temperature $\rho(T)$ becomes linear [Fig. 9(a)]. This behavior is indicative of NFL behavior previously suggested by the specific-heat data. The FL behavior in the low-Ir-doped samples ($x = 0.25$ and 0.5) is recovered for $H = 9$ T [Fig. 9(b)].

IV. CONCLUSIONS

The newly grown single crystals of $Yb_3(Rh_{1-x}T_x)_4Ge_{13}$ (T = Co, Ir) are found to adopt a cubic crystal structure with space group $Pm\bar{3}n$. The ICF magnetic susceptibility behavior, small electronic specific-heat coefficient values γ, and the quadratic temperature dependence of the resistivity at low temperatures show that the Co-doped samples are intermediate-valence systems. By contrast, the γ values are at least one order of magnitude larger (>560 mJ/mol$_{Yb}$ K^2 at $T = 0.4$ K) for $x \geqslant 0.25$ in $Yb_3(Rh_{1-x}Ir_x)_4Ge_{13}$, indicating a crossover towards heavy-fermion behavior with Ir doping. This scenario is supported by other measurements in these crystals, showing Curie-Weiss magnetic susceptibility and Kondo-type local maxima in the $\rho(T)$ data. Antiferromagnetic order at $T_N = 0.96$ K [marked by the vertical line in Fig. 8(e)] in $Yb_3Ir_4Ge_{13}$ is confirmed by $d(MT)/dT$, C_p/T, and $d\rho(T)/dT$. This represents the first known magnetically ordered Yb-based HF in the family of 3-4-13 compounds. The

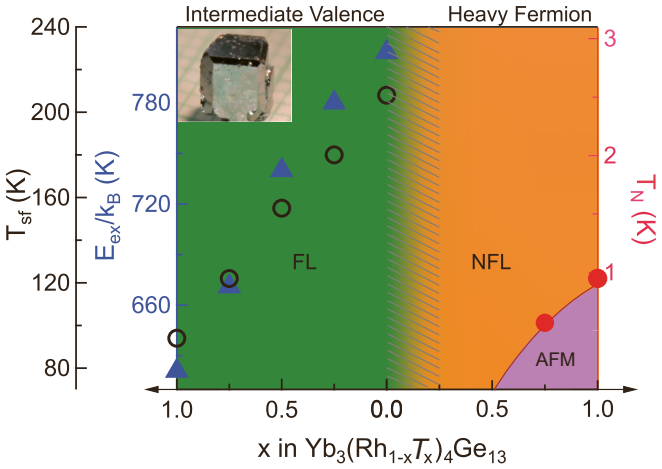

FIG. 10. T-x phase diagram of $Yb_3(Rh_{1-x}T_x)_4Ge_{13}$.

magnetically ordered state is suppressed down to temperatures below 0.35 K by $x_c = 0.5$, as shown in the T-x phase diagram in Fig. 10. The logarithmic behavior of the specific-heat data and the linear resistivity below $x_c = 0.5$ are indicative of a quantum critical point around this composition, accompanied by NFL behavior at $H = 0$. The FL behavior on the HF side of the phase diagram is recovered with application of large magnetic fields [Figs. 6(b)–6(d) and 9].

To investigate the possibility of a spin pseudogap similar to what was recently revealed by nuclear magnetic resonance (NMR) in $YbPtGe_2$ [39,50], NMR measurements on $Yb_3(Rh_{1-x}Co_x)_4Ge_{13}$ are currently underway. Pressure may be used to drive the ICF compounds $Yb_3(Rh_{1-x}Co_x)_4Ge_{13}$ towards the local-moment limit, as a shrinking unit cell may be conducive to a nonmagnetic (large) Yb^{2+} to magnetic (small) Yb^{3+} transition. In turn, the magnetic state in $Yb_3(Rh_{1-x}Co_x)_4Ge_{13}$ under pressure may be tuned towards a QCP, and this is the subject of an ongoing study.

ACKNOWLEDGMENTS

This work at Rice University was supported by the Gordon and Betty Moore Foundation EPiQS initiative through grant GBMF4417 and the Welch Foundation. J. Y. C. acknowledges NSF DMR-1360863.

[1] P. Gegenwart, T. Westerkamp, C. Krellner, Y. Tokiwa, S. Paschen, C. Geibel, F. Steglich, E. Abrahams, and Q. Si, Science **315**, 969 (2007).
[2] J. Paglione, T. A. Sayles, P.-C. Ho, J. R. Jeffries, and M. B. Maple, Nat. Phys. **3**, 703 (2007).
[3] E. Morosan, S. L. Bud'ko, Y. A. Mozharivskyj, and P. C. Canfield, Phys. Rev. B **73**, 174432 (2006).
[4] F. Steglich, J. Aarts, C. D. Bredl, W. Lieke, D. Meschede, W. Franz, and H. Schäfer, Phys. Rev. Lett. **43**, 1892 (1979).
[5] T. Mazet, D. Malterre, M. Francois, C. Dallera, M. Grioni, and G. Monaco, Phys. Rev. Lett. **111**, 096402 (2013).
[6] F. Canepa, S. Cirafici, F. Merlo, and A. Palenzona, J. Magn. Magn. Mater. **118**, 182 (1993).
[7] Y. Muro, K. Yamane, M.-S. Kim, T. Takabatake, C. Godart, and P. Rogl, J. Phys. Soc. Jpn. **72**, 1745 (2003).
[8] E. Bauer, R. Hausert, E. Gratz, D. Gignoux, D. Schmitt, and J. Sereni, J. Phys. Condens. Matter **4**, 7829 (1992).
[9] E. Bauer, Le Tuan, R. Hauser, E. Gratz, T. Holubar, G. Hilscher, H. Michor, W. Perthold, C. Godart, E. Alleno, and K. Hiebl, Phys. Rev. B **52**, 4327 (1995).
[10] B. K. Alami-Yadria, H. Wilhelm, and D. Jaccard, Eur. Phys. J. B **6**, 5 (1998).
[11] G. Knebel, D. Braithwaite, G. Lapertot, P. C. Canfield, and J. Flouquet, J. Phys. Condens. Matter **13**, 10935 (2001).
[12] O. Trovarelli, C. Geibel, S. Mederle, C. Langhammer, F. M. Grosche, P. Gegenwart, M. Lang, G. Sparn, and F. Steglich, Phys. Rev. Lett. **85**, 626 (2000).
[13] E. D. Mun, S. L. Bud'ko, C. Martin, H. Kim, M. A. Tanatar, J.-H. Park, T. Murphy, G. M. Schmiedeshoff, N. Dilley, R. Prozorov, and P. C. Canfield, Phys. Rev. B **87**, 075120 (2013).
[14] P. Gegenwart, Q. Si, and F. Steglich, Nat. Phys. **4**, 186 (2008).
[15] N. D. Mathur, F. M. Grosche, S. R. Julian, I. R. Walker, D. M. Freye, R. K. W. Hasewimmer, and G. G. Lonzarich, Nature (London) **394**, 39 (1998).
[16] H. v. Löhneysen, T. Pietrus, G. Portisch, H. G. Schlager, A. Schröder, M. Sieck, and T. Trappmann, Phys. Rev. Lett. **72**, 3262 (1994).
[17] E. Svanidze, L. Liu, B. Frandsen, B. D. White, T. Besara, T. Goko, T. Medina, T. J. S. Munsie, G. M. Luke, D. Zheng, C. Q. Jin, T. Siegrist, M. B. Maple, Y. J. Uemura, and E. Morosan, Phys. Rev. X **5**, 011026 (2015).
[18] A. Steppke, R. Kuchler, S. Lausberg, E. Lengyel, L. Steinke, R. Borth, T. Lühmann, C. Krellner, M. Nicklas, C. Geibel, F. Steglich, and M. Brando, Science **339**, 933 (2013).
[19] J. P. Remeika, G. P. Espinosa, A. S. Cooper, H. Barz, J. M. Rowel, D. B. McWhan, J. M. Vandenberg, D. E. Moncton, Z. Fisk, L. D. Wolf, H. C. Hamaker, M. B. Maple, G. Shirane, and W. Thomlinson, Solid State Commun. **34**, 923 (1980).
[20] B. Lloret, C. R. Acad. Sci. Paris **303**, 1193 (1986).
[21] G. P. Espinosa, Mater. Res. Bull. **15**, 791 (1980).
[22] K. Ghosh, S. Ramakrishnan, and G. Chandra, Phys. Rev. B **48**, 10435 (1993).
[23] L. E. Klintberg, S. K. Goh, P. L. Alireza, P. J. Saines, D. A. Tompsett, P. W. Logg, J. Yang, B. Chen, K. Yoshimura, and F. M. Grosche, Phys. Rev. Lett. **109**, 237008 (2012).
[24] Y. Mudryk, A. Grytsiv, P. Rogl, C. Dusek, A. Galatanu, E. Idl, H. Michor, E. Bauer, C. Godart, D. Kaczorowski, L. Romaka, and O. Bodak, J. Phys. Condens. Matter **13**, 7391 (2001).
[25] B. K. Rai and E. Morosan, APL Mater. **3**, 041511 (2015).
[26] C. Israel, E. M. Bittar, O. E. Agüero, R. R. Urbano, C. Rettori, I. Torriani, P. G. Pagliusoa, N. O. Moreno, J. D. Thompson, M. F. Hundley, J. L. Sarrao, and H. A. Borges, Physica B (Amsterdam, Neth.) **359-361**, 251 (2005).

[27] A. L. Cornelius, A. D. Christianson, J. L. Lawrence, V. Fritsch, E. D. Bauer, J. L. Sarrao, J. D. Thompson, and P. G. Pagliuso, Physica B (Amsterdam, Neth.) **378–380**, 113 (2006).
[28] A. Ślebarski, B. D. White, M. Fijalkowski, J. Goraus, J. J. Hamlin, and M. B. Maple, Phys. Rev. B **86**, 205113 (2012).
[29] M. F. Hundley, J. L. Sarrao, J. D. Thompson, R. Movshovich, M. Jaime, C. Petrovic, and Z. Fisk, Phys. Rev. B **65**, 024401 (2001).
[30] S. Takayanagi, H. Sato, T. Fukuhara, and N. Wada, Physica B (Amsterdam, Neth.) **199-200**, 49 (1994).
[31] C. P. Yang, Y. H. Chen, H. Wang, C. Nagoshi, M. Kohgi, and H. Sato, Appl. Phys. Lett. **92**, 092504 (2008).
[32] A. M. Strydom, Acta Phys. Pol. A **126**, 318 (2014).
[33] A. M. Strydom, N. Oeschler, and F. Steglich, Physica B (Amsterdam, Neth.) **403**, 746 (2008).
[34] B. K. Rai, I. W. H. Oswald, J. K. Wang, G. T. McCandless, J. Y. Chan, and E. Morosan, Chem. Matter. **27**, 2488 (2015).
[35] A. C. Larson and R. B. Von Dreele, Los Alamos National Laboratory, Report No. LAUR 86-748, 2004 (unpublished).
[36] R. D. Shannon, Acta Crystallogr., Sect. A **32**, 751 (1976).
[37] G. Venturini, M. Méot-Meyer, B. Malaman, and B. Roques, J. Less Common Met. **113**, 197 (1985).
[38] B. C. Sales and D. K. Wohlleben, Phys. Rev. Lett. **35**, 1240 (1975).
[39] R. Gumeniuk, R. Sarkar, C. Geibel, W. Schnelle, C. Paulmann, M. Baenitz, A. A. Tsirlin, V. Guritanu, J. Sichelschmidt, Y. Grin, and A. Leithe-Jasper, Phys. Rev. B **86**, 235138 (2012).
[40] A. Kowalczyk, M. Falkowski, and T. Tolinski, J. Appl. Phys. **107**, 123917 (2010).
[41] E. E. Havinga, K. H. J. Buschow, and H. J. van Daal, Solid State Commun. **13**, 621 (1973).
[42] E. Bauer, R. Hauser, A. Galatanu, H. Michor, G. Hilscher, J. Sereni, M. G. Berisso, P. Pedrazzini, M. Galli, F. Marabelli, and P. Bonville, Phys. Rev. B **60**, 1238 (1999).
[43] E. Bauer, R. Hauser, L. Keller, P. Fischer, O. Trovarelli, J. G. Sereni, J. J. Rieger, and G. R. Stewart, Phys. Rev. B **56**, 711 (1997).
[44] P. Gegenwart, F. Kromer, M. Lang, G. Sparn, C. Geibel, and F. Steglich, Phys. Rev. Lett. **82**, 1293 (1999).
[45] G. R. Stewart, Rev. Mod. Phys. **73**, 797 (2001).
[46] P. Gegenwart, Y. Tokiwa, T. Westerkamp, F. Weickert, J. Custers, J. Fersti, C. Krellner, C. Geibel, P. Kerschl, K.-H. Müller, and F. Steglich, New J. Phys. **8**, 171 (2006).
[47] N. Takeda and M. Ishikawa, J. Phys. Condens. Matter **13**, 5971 (2001).
[48] J. R. Jeffries, N. A. Frederick, E. D. Bauer, H. Kimura, V. S. Zapf, K.-D. Hof, T. A. Sayles, and M. B. Maple, Phys. Rev. B **72**, 024551 (2005).
[49] M. E. Fisher, Philos. Mag. **7**, 1731 (1962).
[50] R. Sarkar, R. Gumeniuk, A. Leithe-Jasper, W. Schnelle, Y. Grin, C. Geibel, and M. Baenitz, Phys. Rev. B **88**, 201101(R) (2013).